SERS Efficiencies of Micrometric Polystyrene Beads Coated with Gold and Silver Nanoparticles: The Effect of Nanoparticle Size

ARTICLE *in* JOURNAL OF OPTICS · JUNE 2015

Impact Factor: 2.01

9 AUTHORS, INCLUDING:

Nicolas Pazos-Perez

University of Bayreuth

39 PUBLICATIONS **772** CITATIONS

SEE PROFILE

Neus G Bastús

Catalan Institute of Nanoscience and Nano…

33 PUBLICATIONS **1,089** CITATIONS

SEE PROFILE

Ramón A Alvarez-Puebla

Catalan Institution for Research and Advan…

139 PUBLICATIONS **4,410** CITATIONS

SEE PROFILE

Luca Guerrini

Medcom Advance SA

42 PUBLICATIONS **603** CITATIONS

SEE PROFILE

IOP Publishing Journal of Optics
J. Opt. 17 (2015) 114012 (9pp) doi:10.1088/2040-8978/17/11/114012

Invited Article

SERS efficiencies of micrometric polystyrene beads coated with gold and silver nanoparticles: the effect of nanoparticle size

Bernat Mir-Simon[1,2], Judit Morla-Folch[1,4], Patricia Gisbert-Quilis[3], Nicolas Pazos-Perez[1,4], Hai-nan Xie[1], Neus G Bastús[5], Víctor Puntes[5,6], Ramon A Alvarez-Puebla[1,4,6] and Luca Guerrini[1,4]

[1] Medcom Advance SA, Viladecans Business Park, Edificio Brasil, C/Bertran i Musitu, 83-85, E-08840 Viladecans (Barcelona), Spain
[2] Department of Surgery, UD-Vall d'Hebron School of Medicine, Universitat Autònoma de Barcelona, E-08035 Barcelona, Spain
[3] Université Paris-Sud, Building 308, F-91405 Orsay, France
[4] Universitat Rovira i Virgili and Centro Tecnológico de la Química de Cataluña (CTQC), Carrer de Marcel·lí Domingo s/n, E-43007 Tarragona, Spain
[5] Institut Català de Nanociència i Nanotecnologia (ICN2), Campus UAB, E-08193 Bellaterra (Barcelona), Spain
[6] ICREA, Passeig Lluís Companys 23, E-08010 Barcelona, Spain

E-mail: luca.guerrini@ctqc.org

Received 21 April 2015, revised 28 May 2015
Accepted for publication 29 May 2015
Published 23 October 2015

Abstract

Rapid advances in nanofabrication techniques of reproducibly manufacturing plasmonic substrates with well-defined nanometric scale features and very large electromagnetic enhancements paved the way for the final translation of the analytical potential of surface-enhanced Raman scattering (SERS) to real applications. A vast number of different SERS substrates have been reported in the literature. Among others, discrete particles consisting of an inorganic micrometric or sub-micrometric core homogeneously coated with plasmonic nanoparticles stand out for their ease of fabrication, excellent SERS enhancing properties, long-term optical stability and remarkable experimental flexibility (manipulation, storage etc). In this article, we performed a systematic experimental study of the correlation between the size of quasi-spherical gold and silver nanoparticle and the final optical property of their corresponding assembles onto micrometric polystyrene (PS) beads. The size and composition of nanoparticles play a key role in tuning the SERS efficiency of the hybrid material at a given excitation wavelength. This study provides valuable information for the selection and optimization of the appropriate PS@NPs substrates for the desired applications.

Keywords: surface-enhanced Raman scattering, plasmonic, nanoparticles, polystyrene microparticles

Introduction

Almost 40 years after the initial discovery of the surface-enhanced Raman scattering (SERS) phenomenon [1], spectacular advances in the development of rationally designed metallic substrates with uniform, reproducible and optimized plasmonic response [2] played a major role in the final translation of the analytical potential of SERS to real applications. As a result, in the last decade we witnessed an exponential increase of applications across many fields of

science [3–9]. Nonetheless, traditional gold and silver colloids prepared via wet chemical methods, such as the well-known Lee-Meisel [10] and Turkevich [11] methods, still remain the most common type of SERS-active materials. In fact, these substrates offer several advantages such as simple and inexpensive syntheses, versatility, ease of manipulation and, when aggregated into plasmonic clusters, high SERS activity due to the concentration of extremely intense electromagnetic fields at the interparticle gaps (hot-spots) [12, 13]. Usually, SERS experiments based on these colloids are either performed in suspension by using long-working distance objectives to acquire highly averaged SERS spectra ('macro' set-up) or upon deposition of the nanoparticles onto solid substrates (this experimental 'micro' set-up normally provides lower detection limits to the detriment of signal reproducibility) [14]. However, these simple colloidal systems suffer from intrinsic limitations. In particular, we highlight the limited colloidal stability, which can be easily compromised when analytes adsorbed onto the nanoparticle in suspension. Addition of stabilizing agents to overcome this issue can, on the other hand, severely limits the access of the target molecules to the metal surface. Furthermore, random aggregation of nanoparticles has shown to provide very large SERS enhancements but with limited stability and reproducibility due to the poor control in cluster size and uniformity in terms of interparticle spacing and geometry. Additionally, SERS measurements with colloidal systems normally require relatively high nanoparticle-to-analyte molecules ratios to investigate a sufficient number of particles/clusters per unit volume in suspension (under the average SERS regime) or deposited onto a solid platform. As a result, the analyte molecules are 'diluted' over a larger metallic surface area, which consequently increases the minimum concentration of the target to obtain a distinguishable SERS spectrum.

Our group has been largely involved in the investigations aimed at the rational design of novel SERS substrates, with long-term stability and large enhancement efficiency [15–18]. Among others, we have designed and produced discrete particles consisting of an inorganic micrometric or submicrometric core homogenously coated with plasmonic nanoparticles which possesses several important positive features of simple metal colloids (simple fabrication methods and normally available in all spectroscopy laboratories; facile surface-functionalization, high SERS activity in their aggregated forms etc) while introducing dramatic improvements in terms of stability, signal reproducibility and experimental flexibility [19–21]. These hybrid materials act as robust microscopic carriers of large ensembles of interparticle hot-spots concentrated in their external shell. The tens of thousands of nanoparticles anchored to the polymeric surface provide, in addition to high SERS activity via interparticle coupling, a highly averaged plasmonic response that ensures the great homogeneity within the bead to bead Raman signal enhancing [20, 22, 23]. Therefore, average SERS measurements in suspension can be performed at very low bead concentration in suspension [21], and single-bead analysis onto a solid surface (micro set-up) is very straightforward and simple since the beads are plainly visible with a 50× objective. As previously mentioned, it is important to stress the extreme experimental flexibility offered by these supports. In fact, their intrinsic resistance against aggregation allows the desired manipulations (i.e. centrifugations, redispersions, surface functionalization, changes in ionic strengths as well as solvents etc) with no risk of perturbation of their SERS response.

In this article, we systematically investigate the correlation between the size of quasi-spherical gold (Au NPs) and silver nanoparticles (Ag NPs) in suspension and the final optical property of their corresponding assembles onto 3 μm polystyrene (PS) beads. Colloids were synthesized via standard wet chemical methods using citrate and/or ascorbic acid as a stabilizing/reducing agent to yield nanoparticles with similar surface chemistry (surface properties largely determine the adhesion of the nanoparticles onto the beads as well as the affinity of analytes for silver/gold). The SERS activity of each material was characterized by using thiophenol (TP) as a Raman label and some of the most common excitation wavelengths used nowadays in SERS spectroscopy (532, 633 and 785 nm). The experimental results indicate that size and composition of nanoparticles play a key role in tuning the SERS efficiency of the hybrid material at a given excitation wavelength, providing valuable information for the selection and optimization of the appropriate PS@NPs substrates for the desired applications.

Experiment

Synthesis of Ag NPs

To synthesize spherical-like Ag NPs with average diameter in the 40–120 nm range, we used a modified protocol based on the combination of previously reported approaches [10, 24–26]. Briefly, 250 mL of milli Q water were heated under vigorous stirring. A condenser was used to prevent solvent evaporation. Adequate amounts of aqueous solutions of trisodium citrate (0.1 M) and ascorbic acid (0.1 M) were consecutively added to the boiling water. After 1 min, 0.1 M of $AgNO_3$ solution was injected into the reaction vessel under vigorous stirring. In some cases $MgSO_4$ was also used, and the $AgNO_3$ and $MgSO_4$ aliquots were first premixed (stock solutions of $AgNO_3$ 0.1 M and $MgSO_4$ 0.1 M) and incubated at room temperature for 5 min before the injection. The color of the solution quickly changed from colorless to yellow and gradually changed into orange or white-greenish depending on the nanoparticle size. Boiling was continued for 1 h under stirring to ensure the completeness of the reaction. The size of the Ag NPs was controlled by adjusting the concentrations of the different reactants. As a general trend, by adding $MgSO_4$ and increasing its concentration, the size of Ag NPs increases. Similar trend is also observed when the ascorbic acid or the $AgNO_3$ were increased. Table S1 describes the amount of reactants used in each synthesis whereas figure S1 illustrates the histogram of Ag NP size distribution and representative transmission electron microscopy (TEM) images of the dried colloids.

Synthesis of Au NPs

Small gold nanoparticles (AuNPs) of ~15 nm diameter were prepared according to the Turkevich-Frens preparation method [11, 27]. Briefly, $HAuCl_4$ trihydrate (15 mg) was dissolved in milli-Q water (150 mL) and heated to boil. An aqueous solution of trisodium citrate (1% v/v, 4.5 mL), previously warmed to ca. 70–75 °C was then quickly added, and the mixture was refluxed for further 30 min until the solution turned ruby red in color. The solution was then allowed to cool to room temperature under vigorous stirring for several hours.

Large gold nanoparticles of ~55, ~65, ~100 and ~165 nm were prepared by following the previously reported seeded growth method [28]. Briefly, a solution of 2.2 mM sodium citrate in milli-Q water (150 mL) was heated with a heating mantle in a 250 mL three-necked round-bottomed flask for 15 min under vigorous stirring. A condenser was utilized to prevent the evaporation of the solvent. After boiling had commenced, 1 mL of $HAuCl_4$ (0.25 M) was injected. The color of the solution changed from yellow to bluish gray and then to soft pink in 10 min. The resulting particles are coated with negatively charged citrate ions and hence are well suspended in H_2O. Once the synthesis was finished the solution was cooled down to 90 °C and 1 mL of $HAuCl_4$ solution (0.25 M) was injected. After 30 min the reaction was finished. This process was repeated twice. After that, the sample was diluted by extracting 50 mL of sample and adding 45 mL of milli-Q water and 5 mL of 60 mM of sodium citrate. This solution was then used as the seed solution and the process was repeated again.

Assembly of PS@Au microbeads

PS microbeads of 3 μm diameter (0.5 mL of a 100 mg mL^{-1} suspension) were first wrapped with alternating polyelectrolyte monolayers using the layer-by-layer (LbL) electrostatic self-assembly protocol [21, 29, 30]. Four alternate layers were deposited: polystyrenesulfonate (PSS, Mw = 1000 000), polyethylenimine branched (PEI, Mw = 25 000), PSS, and, finally, PEI. PS microbeads (0.5 mL of a 100 mg mL^{-1} suspension) were added to 25 mL of a 2 mg mL^{-1} PSS aqueous solution containing 0.5 M of NaCl. After 30 min of sonication and 2 h of agitation, the PS microbeads were extensively washed with milli-Q water and centrifuged (5800 rpm, 20 min). The same protocol (concentrations, elapsed times, and washing protocol) was carried out for depositing subsequent layers of PEI, PSS and PEI polyelectrolytes. Finally, the PS beads were redispersed in 10 mL of milli-Q water (final concentration 5 mg mL^{-1}).

The adsorption of the particles onto the functionalized beads was carried out by adding 50 μL of PS beads (5 mg mL^{-1}) to 20 mL of Ag colloids ([Ag] = 0.15 mM) and 20 mL Au colloids (0.1 mM). After 15 min of sonication, the PS@Ag and PS@Au beads were left under gently shaking for two hours and then left to deposit overnight. The clear supernatant was removed and the process was repeated until reaching the full bead saturation (i.e. when the supernatant remained visibly colored). The mixtures were washed first three times by centrifugation (3000 rpm, 30 min) and then three times by decantation with milli-Q water. The beads were redispersed in 500 μL of milli-Q water (final PS bead concentration of 0.5 mg mL^{-1}).

SERS characterization

For SERS characterization of Ag NPs, 500 μL of each colloidal suspension was passivated by addition of 30 μL of a 2% w/w aqueous solution of polyethylene glycol sorbitan monolaurate, a nonionic surfactant (Tween® 20) in order to prevent unwanted aggregation of the particles upon addition of the Raman probe. Then, TP was added to a final concentration of 1×10^{-6} M and the samples were left aging overnight. Finally, the samples were centrifuged and redispersed in 60 μL of milli-Q water. The same functionalization protocol was applied for Au nanoparticles, but in this case the final TP concentration in the samples were 7×10^{-7} M before the final centrifugation step. The chosen [NP]/[TP] ratio was carefully selected to afford a sub-monolayer coverage of the Raman probe onto the metal surface. Thus, the SERS performance of the different colloids can be safely ascribed only to the individual nanoparticle properties whereas the number of TP molecules investigated remains constant and the uncontrolled formation of hot-spots in nanoparticle clusters is avoided.

For SERS characterization of the PS@Ag and Au beads, 100 μL of PS@Ag and Au (0.5 mg mL^{-1} of PS beads) were mixed with 1 mL of an ethanolic solution of 10^{-3} M of TP. After 2 h aging, the beads were submitted to one centrifugation/washing cycle with ethanol and two centrifugation/washing cycles with milli-Q. The samples were finally redispersed in 100 μL of milli-Q water and investigated by SERS under the macro condition using a long working distance objective. For micro SERS measurements, 10 μL of the different samples of coated PS@Ag and Au beads was deposited on a clean glass slide. Each sample was prepared at least twice at the same conditions, and at least 15 different beads were measured for each sample to ensure reproducibility.

Instrumentation

SERS experiments were conducted using a Renishaw InVia Reflex confocal microscope equipped with a 1200 grooves mm^{-1} grating for the NIR wavelengths, additional band-pass filter optics, and a CCD camera. Spectra were acquired using 532, 633 and 785 nm laser excitations either in macro condition by focusing the laser onto the sample with a long working distance objective or in micro set-up by using a 50× objective (N.A. 0.75). UV–vis spectra were recorded using a Thermo Scientific Evolution 201 UV–visible spectrophotometer. Environmental scanning electron microscopy was performed with a JEOL 6400 scanning electron microscope. TEM was performed with a JEOL JEM-1011 transmission electron microscope.

Results and discussion

The preparation of PS beads decorated with Ag or Au nanoparticles (PS@Ag and PS@Au, respectively) was performed via LbL assembly protocol, as previously described [21]. Negatively charged PSS and positively charged branched-PEI were alternatively deposited onto PS beads of 3 μm diameter to form a final dense external layer of PEI. In a second step, large excesses of the negatively charged Ag or Au colloids were left to adhere via electrostatic interaction to the external positively charged PEI layer of the PS beads, saturating the microparticle surfaces. Finally, the final composite PS@nanoparticle structures were extensively washed to remove the unbound nanoparticles. All Ag and Au colloids were prepared via standard chemical methods using citrate and/or ascorbic acid as reducing agents and citrate as a stabilizing agent. We carefully avoided the use of surfactants or polymers such as CTAB or PVP with high affinity toward the metal surfaces that would have dramatically altered the surface chemistry of the nanostructures thus, their adhesion onto the PS surface as well as the accessibility of the Raman label to the metallic surface [26, 31].

Ag and Au colloids

Monodispersed quasi-spherical Ag NPs with average diameters of 39, 49, 56, 70, 92 and 121 nm were prepared using a modified protocol based on previously reported strategies [10, 24–26]. Figure S1 shows representative TEM images of each colloids together with their histograms of size distribution. The size of Ag NPs was controlled by adjusting the concentrations of the different reactants in milli-Q water (trisodium citrate, ascorbic acid, silver nitrate and magnesium sulfate), as reported in table S1.

Figure 1(A) shows the normalized extinction spectra of the different Ag colloids in suspension. The spectra reveal the characteristic localized-surface plasmon resonances (LSPRs) of spherical Ag NPs centered in the violet spectral range, which progressively shift to the higher wavelengths and broaden when the average size is increased. High-order LSPR modes, such as the quadrupolar resonance appearing as a blue-shifted shoulder at ca. 360 nm for small nanoparticles, become more and more evident as the size increased, until reaching a magnitude even higher than the dipolar resonance for nanoparticles >100 nm in diameter [12]. In fact, as the nanoparticle size increases, light cannot polarize homogeneously and the field is no longer uniform throughout the NP, which results in the phase retardation effect. As a consequence, a red-shift and broadening of the dipolar resonance is observed in the larger particles along with the appearance of higher-order modes [32, 33].

The Raman enhancing ability of the different monodispersed colloidal suspensions was evaluated by adding TP as a Raman probe. TP is commonly used as a molecular probe for characterizing the SERS properties of plasmonic substrates. This is because, on the one hand, its –SH group shows very high affinity toward noble metal surfaces, which leads to the formation of covalent sulfur-metal bonds. On the other hand, TP has also a high Raman cross-section, then providing intense SERS signals with a well-defined vibrational fingerprint. Previously to the addition of TP, the colloids were passivated with Tween 20, a nonionic surfactant. Differently to surfactants such as CTAB or PVP, Tween 20 simply physisorbes on the metallic surface providing an effective steric protection that prevents the uncontrolled formation of nanoparticle clusters due to the adsorption of TP molecules perturbing the colloidal stability [34, 35]. For a meaningful comparison of the enhancing performance of colloids with different nanoparticle size and concentration (i.e. different

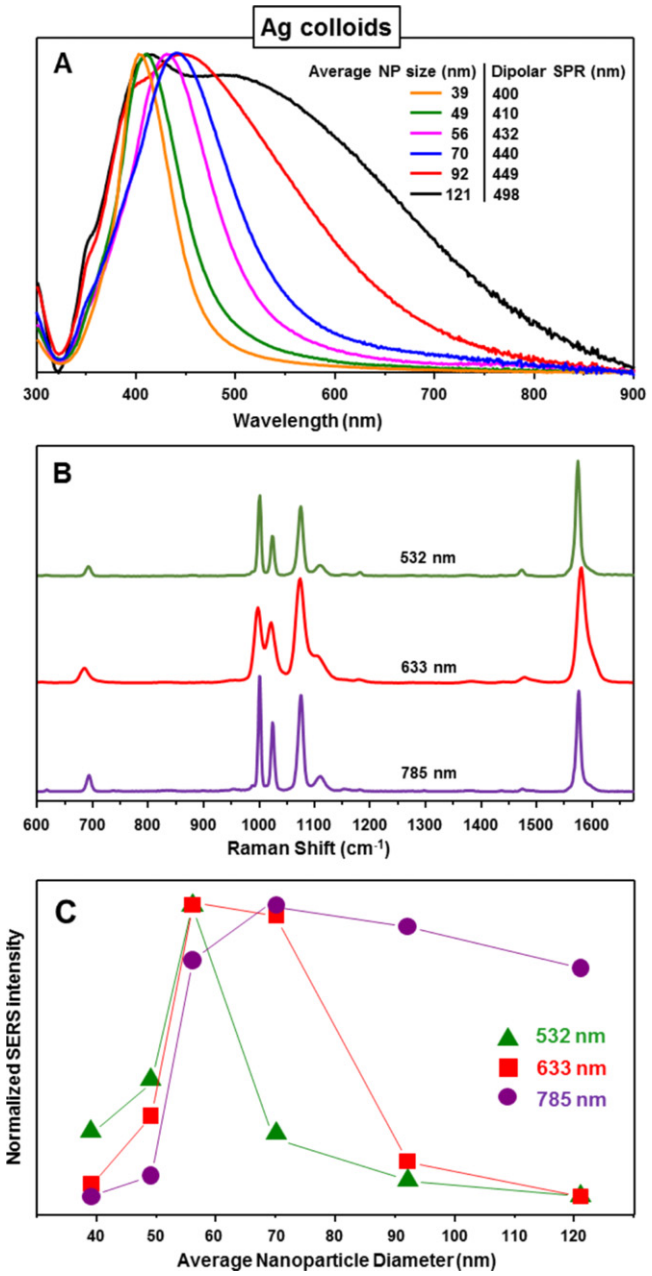

Figure 1. (A) Normalized extinction spectra of Ag colloids. (B) SERS spectra of TP on Ag(56 nm)NPs colloids at 532, 633 and 785 nm. (C) Normalized SERS intensities of the TP band at 1073 cm^{-1} on silver colloids at 532, 633 and 785 nm for different nanoparticle size.

silver surface areas available for TP adhesion), we added a fixed amount of Raman label providing a sub-monolayer coverage for the all investigated samples rather than saturating the metallic surfaces. In this way, the number of molecules contributing to the vibrational spectra is constant and, thus, to a first approximation the final SERS intensity is solely associated to the Raman signal enhancing properties of the different nanoparticles in suspension. The validity of this approximation also lies in the fact that the field enhancement over nanoparticles of spherical geometry shows a relatively good uniformity [12]. Figure 1(B) illustrates the characteristic SERS spectra of TP on Ag colloids acquired at 532 nm, 633 nm and 785 nm excitation respectively. The spectra are dominated by the intense ring breathing bands at ca. 999, 1023 and 1073 cm^{-1} (the last one coupled with νCS) and the CC stretching vibrations at ca. 1574 cm^{-1} [36]. The comparison of the different SERS efficiency provided by the Ag colloids is reported in figure 1(C), where the intensity of the TP band at 1073 cm^{-1} is plotted against the average nanoparticle size. It is known that for the individual quasi-spherical nanoparticles, it exists a qualitative connection between the extinction and SERS enhancement [37] (whereas no correlation is observed for plasmonically interacting objects [37, 38]). For Ag nanospheres, the most intense electromagnetic fields occur when the laser excitation is centered at the LSPR maxima, even though the long tail distribution of the SERS enhancements allows to obtain large signal intensification in spectral regions where the plasmon resonances are very weak [12, 37]. Thus, red-shift of the LSPRs maxima of Ag colloids toward the spectral position of the excitation sources by increasing the nanoparticle sizes is expected to improve the interaction of the external field with the plasmon resonances. On the other hand, LSPRs significantly broaden due to radiation losses when the NP size is increased above ca. 50 nm diameter [12]. Therefore, the optimal nanoparticle size that maximizes the SERS enhancement is a compromise between these two opposite factors and depends, among others, on the excitation wavelength. This is clearly shown by the experimental data illustrated in figure 1(C) which highlights how the optimum nanoparticle size approximately increases as we shift the excitation source to longer wavelength, from 532 to 633 nm and finally to 785 nm.

Highly monodispersed quasi-spherical citrate-stabilized gold nanoparticles of different average sizes (15, 55, 65, 100 and 165 nm) were produced following a seeded growth strategy based on the classical Turkevich/Frens reaction (figure S2) [39]. The normalized extinction spectra of the corresponding colloidal suspensions are illustrated in figure 2(A), where we observe the characteristic red-shift and broadening of the LSPR for larger nanoparticle diameters [12]. Differently to silver, quadrupolar resonance modes are only observed for the particle size above 100 nm [33], as clearly revealed by the shoulder at shorter wavelengths appearing in the 165 nm gold colloids. Figure 2(B) shows the SERS spectra of TP on the Au (55 nm) NPs suspensions upon excitation with 633 and 785 nm lasers. Due to the large optical absorption of gold at shorter wavelengths (<600 nm)

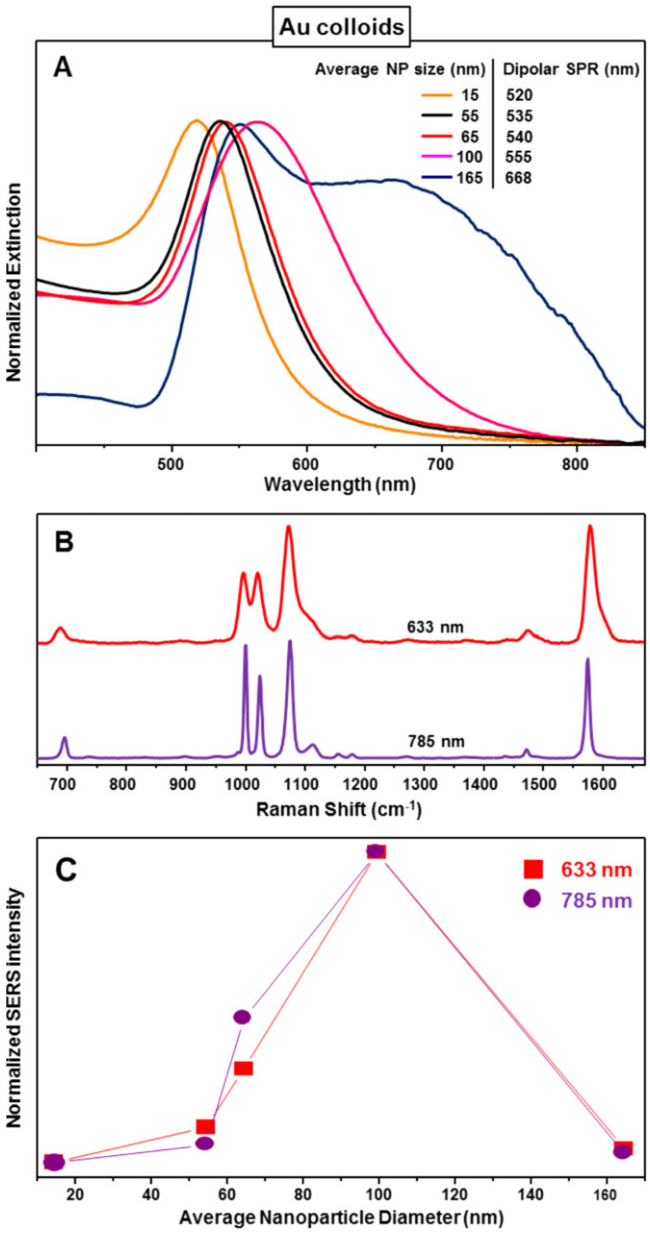

Figure 2. (A) Normalized extinction spectra of Au colloids. (B) SERS spectra of TP on Au(55 nm)NPs colloids at 633 and 785 nm. (C) Normalized SERS intensities of the TP band at 1073 cm^{-1} on gold colloids at 633 and 785 nm for different nanoparticle size.

[12], no distinguishable SERS signal can be collected when illuminating gold nanoparticles with the 532 nm excitation source. As for Ag NPs, the Raman signal enhancing ability of the different monodispersed colloidal suspensions was evaluated by adding a sub-monolayer amount of TP molecules in the presence of Tween 20 as a stabilizing agent. The normalized SERS intensities of the ring breathing band at 1073 cm^{-1} are plotted against the average nanoparticle size in figure 2(C), showing a marked increase of the SERS activity upon enlarging the nanoparticle diameter up to a maximum around 100 nm. This is consistent with previous experimental studies [40, 41]. In fact, incrementing the nanoparticle size causes a red-shift of the LSPR, which maximum is tuned

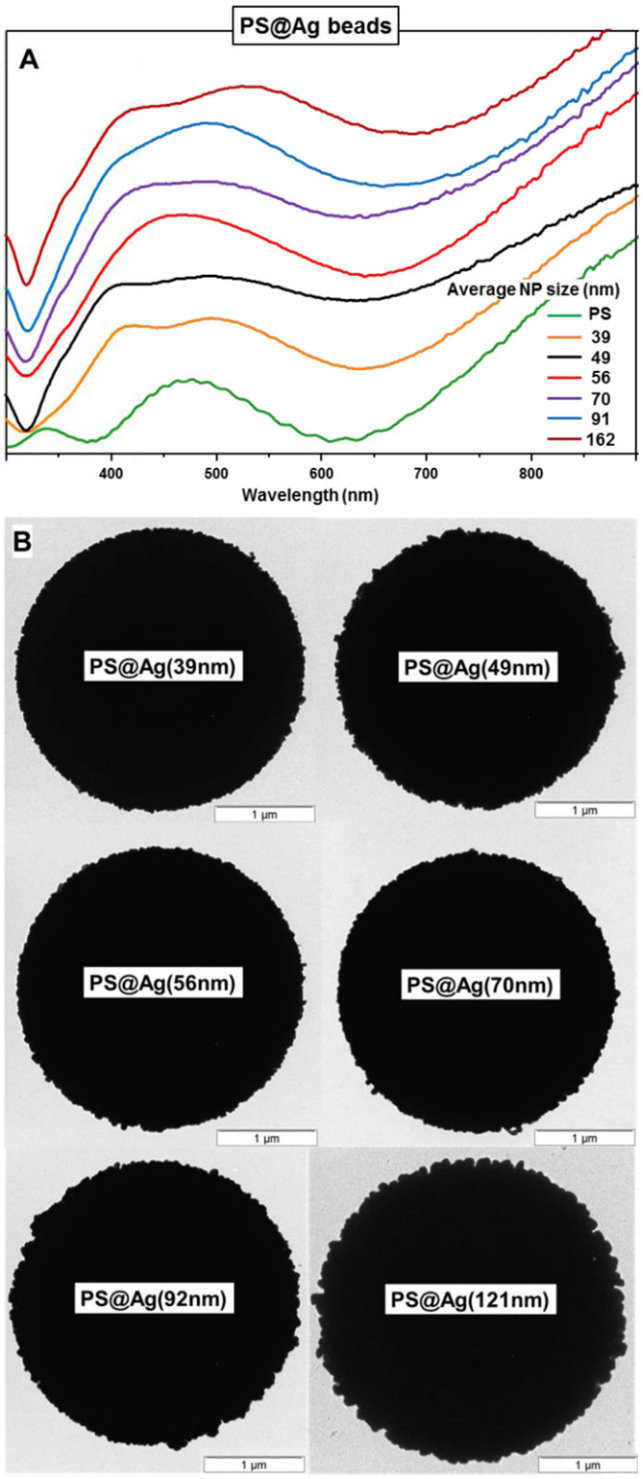

Figure 3. (A) Extinction spectra of PS@Ag composite materials in suspension (normalized and stacked). (B) Representative TEM images of PS@Ag beads.

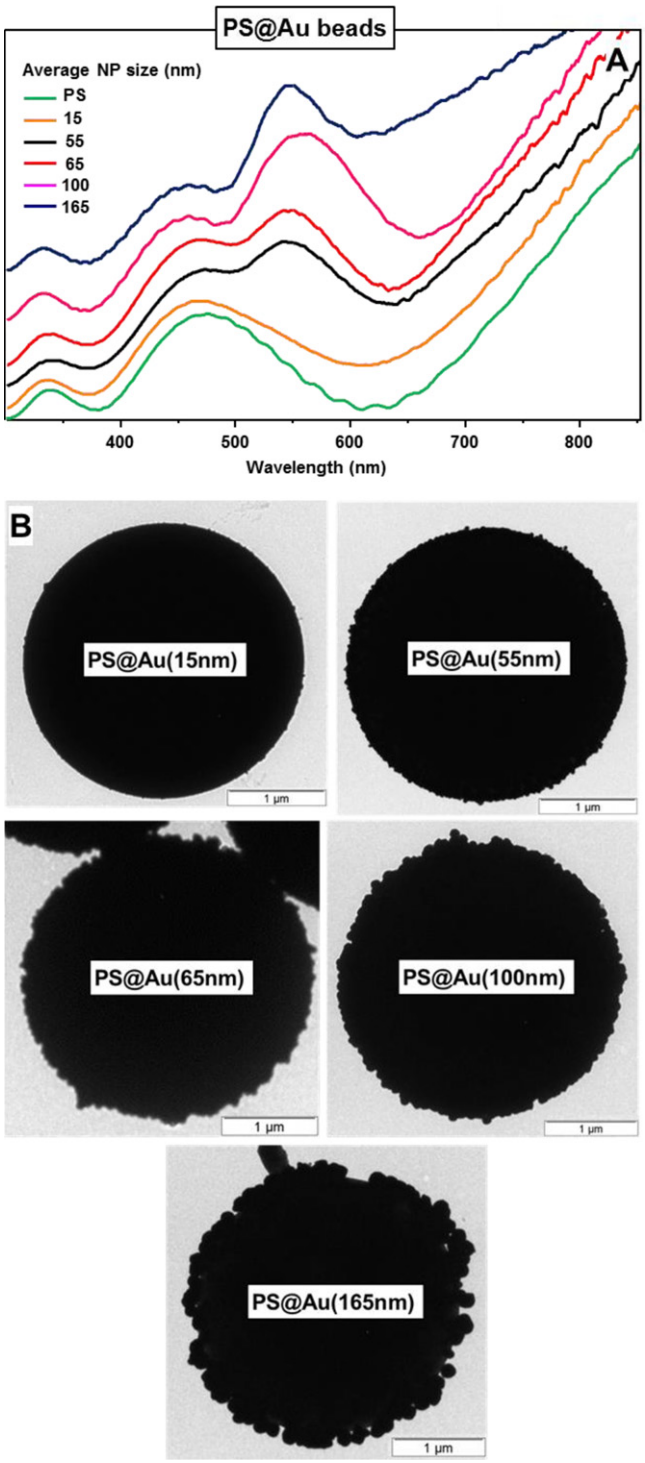

Figure 4. (A) Extinction spectra of PS@Au composite materials in suspension (normalized and stacked). (B) Representative TEM images of PS@Au beads.

closer to the wavelengths of the excitation sources. However, for sizes larger than ca. 100 nm, the radiation damping becomes dominant [12], significantly reducing the electromagnetic fields at the metallic surface, as it can be observed by the poor enhancing performance of the 165 nm gold nanoparticles.

PS@Ag and PS@Au composite materials

Silver and gold nanoparticles were then assembled onto the PS beads until surface saturation (figures 3 and 4, and figure S3). As a result, the plasmonic coupling of the interacting metallic nanoparticles on the bead surface leads to a reshaping of the extinction spectra as well as the alteration of the nanoparticle size-dependent pattern of the SERS response [23].

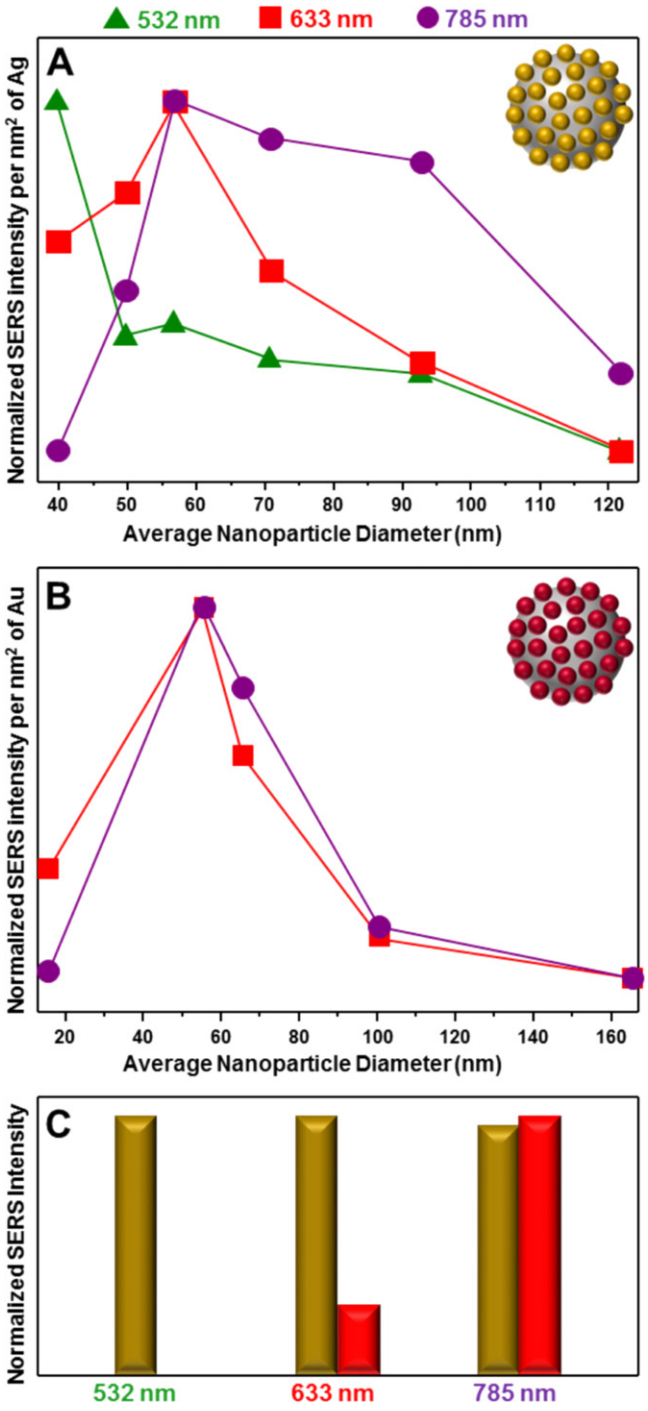

Figure 5. (A) Normalized SERS intensities of the TP band at 1073 cm^{-1} on PS@Ag at 532 nm, 633 nm and 785 nm respectively for different nanoparticle size. (B) Normalized SERS intensities of the TP band at 1073 cm^{-1} on PS@Au at 532 nm, 633 nm and 785 nm respectively for different nanoparticle size. (C) Relative SERS efficiency of PS@Au(55 nm) and PS@Ag(56 nm) at the three excitation wavelengths. In this case, for a specific excitation wavelength, the SERS measurements were performed under the same experimental conditions for both PS@Ag(56 nm) and PS@Au (55 nm); subsequently, the recorded TP SERS intensities (peak height at 1073 cm^{-1}) were normalized to the maximum value.

The extinction spectra of the PS@Ag beads in suspension are shown in figure 3(A). First of all, we notice how the PS core contributes to the overall spectra with a large scattering background, characterized by a well-defined band centered at ca. 470 nm and a long tail at the longer wavelength. Nonetheless, it is possible to recognize two new contributions in the extinction profile of PS@Ag: one blue-shifted with respect to the PS feature at 470 nm and a second broader one in the ca. 500–580 nm range. The latter can be ascribed to the dipolar coupling between individual nanoparticle dipolar LSPRs whereas the resonances appearing at shorter wavelengths can be due to the poor/null plasmonically interacting single nanoparticles and/or the high-order interactions between single-sphere dipolar LSPRs [12].

Similarly, the plasmonic interaction between closely spaced gold nanoparticles is revealed by the change of the extinction spectra (figure 4). We observe a significant red-shift of the plasmon resonances, overlapping the large scattering background of the PS cores, as compared to the original LSPRs of the monodispersed colloids. It is worth noticing that the PS@Au(165 nm) suspension retains a significant amount of unbound Au nanoparticles which were not possible to efficiently remove through the normal sedimentation protocol as for the other samples. This difficulty arises from the fact that the colloidal solution of large AuNPs naturally sediment from solution due to the gravitational force. Thus, the UV–vis spectrum of PS@Au(165 nm) may be significantly biased by the contribution of free gold nanoparticles.

We then investigated the size-dependent profile at different excitation wavelengths of the normalized SERS intensity of PS@Ag and PS@Au samples (figures 5(A) and (B), respectively). The illustrated data were obtained by averaging the SERS response of the beads in suspension investigated with a long working distance objective (macro set-up) and 15 different beads dried onto a glass slide using a 50× objective (micro set-up). This averaging process was performed to minimize the contribution to the final results of experimental uncertainties associated with, for instance, the exact bead concentration in suspension after several centrifugation/washing cycles, the focusing of the laser spot on each beads etc. The SERS activity of the PS@Ag beads was tested by measuring the signal intensity of the TP band at 1073 cm^{-1}. In this case, the beads were fully saturated with the Raman label by exposing them to an excess of TP in ethanolic solution which implies that the number of TP molecules yielding the final SERS spectra differs from sample to sample. Thus, to correct such variations, we express the results in terms of SERS intensities per 1 nm^2 of metallic surface available on the PS coated-bead. This estimation was performed by assuming a full monolayer coating of metallic nanoparticles on top of the PS surface. The results illustrated in figure 5(A) highlights a drastic change of the size-dependent SERS performance of Ag NPs when assembled onto the surface beads as compared to their individual condition in suspension (figure 1(C)). For green laser excitation, the SERS activity decreases with the increase of nanoparticle size, whereas in the case of 633 and 785 nm the SERS performance reaches a maximum for Ag NPs of 56 nm and ca. 56–70 nm, respectively. On the other hand, the averaged and normalized SERS values obtained for PS@Au composites are reported in figure 5(B) against the average nanoparticle diameter. At

both excitation wavelengths, the enhancing performance of the composite materials approximately decreases according to the following order: PS@Au(55 nm) >PS@Au(65 nm) ≫ PS@Au(15 nm) >PS@Au(100 nm) >PS@Au(165 nm).

Finally, in figure 5(C) we compared the relative SERS efficiency of PS@Au_{55} and PS@Ag(56 nm) at the different excitation wavelengths. Silver-based composite provides a much more efficient SERS substrate for shorter wavelengths whereas the enhancement performances of PS@Au_{55} beads become competitive and finally overcome those of PS@Ag (56 nm) at 785 nm. This is associated with the generation of interparticle gap-associated resonances, the most important ones for SERS, which are shifted beyond 600 nm, where the optical absorption of gold is low and both metals (Ag and Au) behave similarly [12].

Conclusions

In summary, we performed a thorough investigation of the correlation between the size of quasi-spherical Ag and Au nanoparticles and the SERS efficiency of the corresponding composite hybrid materials, comprising of a PS micro-core and a dense external layer of interacting nanoparticles. TP was selected as an efficient Raman label for our SERS study. The results show how the enhancing ability of the PS@Ag/Au substrates are strongly determined by the size (and composition) of the individual nanoparticles, and the dependency to the selected excitation wavelength. In the case of PS@Ag composite microparticles, Ag NPs of ca. 39, 56 and 56–70 nm yielded the most efficient substrates at the three investigated excitation wavelengths (532 nm, 633 nm and 785 nm, respectively). On the other hand, for PS@Au, gold nanoparticles of ca. 55 nm diameter resulted the best choice for all laser sources. Regarding the nanoparticle composition, silver-based hybrid beads generated the most intense SERS signals when illuminated with the 532 and 633 nm lasers, whereas under the 785 nm excitation the SERS performances of PS@Au(55 nm) and PS@Ag(56–70) are similar. We believe these findings offer important information to researchers for the fabrication and appropriate selection of the optimum PS@Ag/Au substrates for a different set of potential applications.

Acknowledgments

This work was funded by the Spanish Ministerio de Economia y Competitividad (CTQ2011-23167), the European Research Council (CrossSERS, FP7/2013 329131, PrioSERS FP7/2014 623527) and Medcom Advance SA. N G B and V P acknowledge financial support from the Generalitat de Catalunya (2014-SGR-612), Spanish MICINN (MAT2012-33330) and European Community (EU-FP7) through the FutureNanoNeeds project. N G B thanks the Spanish MICINN for the financial support through the Ramon y Cajal program and European Commission for the Career Integration Grant (CIG)-Marie Curie Action.

References

[1] Fleischmann M, Hendra P J and McQuillan A J 1974 Raman spectra of pyridine adsorbed at a silver electrode *Chem. Phys. Lett.* **26** 163–6
[2] Ko H, Singamaneni S and Tsukruk V V 2008 Nanostructured surfaces and assemblies as SERS media *Small* **4** 1576–99
[3] Alvarez-Puebla R A and Liz-Marzan L M 2012 Traps and cages for universal SERS detection *Chem. Soc. Rev.* **41** 43–51
[4] Alvarez-Puebla R A and Liz-Marzan L M 2012 SERS detection of small inorganic molecules and ions *Angew. Chem., Int. Ed. Engl.* **51** 11214–23
[5] Alvarez-Puebla R A and Liz-Marzan L M 2010 SERS-based diagnosis and biodetection *Small.* **6** 604–10
[6] Schlücker S 2014 Surface-enhanced raman spectroscopy: concepts and chemical applications *Angew. Chem., Int. Ed. Engl.* **53** 4756–95
[7] Golightly R S, Doering W E and Natan M J 2009 Surface-enhanced raman spectroscopy and homeland security: a perfect match? *ACS Nano* **3** 2859–69
[8] Wang Y Q, Yan B and Chen L X 2013 SERS tags: novel optical nanoprobes for bioanalysis *Chem. Rev.* **113** 1391–428
[9] Kim H, Kosuda K M, Van Duyne R P and Stair P C 2010 Resonance raman and surface- and tip-enhanced raman spectroscopy methods to study solid catalysts and heterogeneous catalytic reactions *Chem. Soc. Rev.* **39** 4820–44
[10] Lee P C and Meisel D 1982 Adsorption and surface-enhanced raman of dyes on silver and gold sols *J. Phys. Chem.* **86** 3391–5
[11] Turkevich J, Stevenson P C and Hillier J 1951 A study of the nucleation and growth processes in the synthesis of colloidal gold *Discuss. Faraday Soc.* **11** 55–75
[12] Ru E C L and Etchegoin P G 2009 *Principles of Surface-Enhanced Raman Spectroscopy and Related Plasmonic Effects* (Amsterdam: Elsevier)
[13] Moskovits M 1985 Surface-enhanced spectroscopy *Rev. Mod. Phys.* **57** 783–826
[14] Aroca R 2006 *Surface-Enhanced Vibrational Spectroscopy* (Chichester: Wiley)
[15] Alba M *et al* 2013 Macroscale plasmonic substrates for highly sensitive surface-enhanced Raman scattering *Angew. Chem., Int. Ed. Engl.* **52** 6459–63
[16] Pazos-Perez N, Wagner C S, Romo-Herrera J M, Liz-Marzan L M, de Abajo F J G, Wittemann A, Fery A and Alvarez-Puebla R A 2012 Organized plasmonic clusters with high coordination number and extraordinary enhancement in surface-enhanced raman scattering (SERS) *Angew. Chem., Int. Ed. Engl.* **51** 12688–93
[17] Alvarez-Puebla R A *et al* 2011 Gold nanorods 3d-supercrystals as surface enhanced Raman scattering spectroscopy substrates for the rapid detection of scrambled prions *Proc. Natl Acad. Sci. USA* **108** 8157–61
[18] Sanles-Sobrido M, Exner W, Rodriguez-Lorenzo L, Rodriguez-Gonzalez B, Correa-Duarte M A, Alvarez-Puebla R A and Liz-Marzan L M 2009 Design of SERS-encoded, submicron, hollow particles through confined growth of encapsulated metal nanoparticles *J. Am. Chem. Soc.* **131** 2699–705
[19] Tsoutsi D, Montenegro J M, Dommershausen F, Koert U, Liz-Marzan L M, Perak W J and Alvarez-Puebla R A 2011 Quantitative surface-enhanced Raman scattering ultradetection of atomic inorganic ions: the case of chloride *ACS Nano* **5** 7539–46
[20] Spuch-Calvar M, Rodriguez-Lorenzo L, Morales M P, Alvarez-Puebla R A and Liz-Marzan L M 2009 Bifunctional nanocomposites with long-term stability as SERS optical

accumulators for ultrasensitive analysis *J. Phys. Chem.* C **113** 3373–7
[21] Guerrini L, Rodriguez-Loureiro I, Correa-Duarte M A, Lee Y H, Ling X Y, de Abajo F J G and Alvarez-Puebla R A 2014 Chemical speciation of heavy metals by surface-enhanced Raman scattering spectroscopy: identification and quantification of inorganic- and methyl-mercury in water *Nanoscale* **6** 8368–75
[22] Abalde-Cela S, Hermida-Ramon J M, Contreras-Carballada P, De Cola L, Guerrero-Martinez A, Alvarez-Puebla R A and Liz-Marzan L M 2011 SERS chiral recognition and quantification of enantiomers through cyclodextrin supramolecular complexation *Chem. Phys. Chem.* **12** 1529–35
[23] Lange H, Juárez B H, Carl A, Richter M, Bastús N G, Weller H, Thomsen C, von Klitzing R and Knorr A 2012 Tunable plasmon coupling in distance-controlled gold nanoparticles *Langmuir* **28** 8862–6
[24] Li H, Xia H, Wang D and Tao X 2013 Simple synthesis of monodisperse, quasi-spherical, citrate-stabilized silver nanocrystals in water *Langmuir* **29** 5074–9
[25] Li H, Xia H, Ding W, Li Y, Shi Q, Wang D and Tao X 2014 Synthesis of monodisperse, quasi-spherical silver nanoparticles with sizes defined by the nature of silver precursors *Langmuir* **30** 2498–504
[26] Mir-Simon B, Reche-Perez I, Guerrini L, Pazos-Perez N and Alvarez-Puebla R A 2015 Universal one-pot and scalable synthesis of SERS encoded nanoparticles *Chem. Mater.* **27** 950–8
[27] Frens G 1973 Controlled nucleation for regulation of particle-size in monodisperse gold suspensions *Nat.-Phys. Sci.* **241** 20–2
[28] Bastús N G, Comenge J and Puntes V C 2011 Kinetically controlled seeded growth synthesis of citrate-stabilized gold nanoparticles of up to 200 nm: size focusing versus ostwald ripening *Langmuir* **27** 11098–105
[29] Decher G 1997 Fuzzy nanoassemblies: toward layered polymeric multicomposites *Science* **277** 1232–7
[30] Ahijado-Guzman R, Gomez-Puertas P, Alvarez-Puebla R A, Rivas G and Liz-Marzan L M 2012 Surface-enhanced Raman scattering-based detection of the interactions between the essential cell division ftsZ protein and bacterial membrane elements *ACS Nano* **6** 7514–20
[31] Guerrini L, Jurasekova Z, del Puerto E, Hartsuiker L, Domingo C, Garcia-Ramos J V, Otto C and Sanchez-Cortes S 2013 Effect of metal–liquid interface composition on the adsorption of a cyanine dye onto gold nanoparticles *Langmuir* **29** 1139–47
[32] Myroshnychenko V, Rodriguez-Fernandez J, Pastoriza-Santos I, Funston A M, Novo C, Mulvaney P, Liz-Marzan L M and Garcia de Abajo F J 2008 Modelling the optical response of gold nanoparticles *Chem. Soc. Rev.* **37** 1792–805
[33] Rodríguez-Fernández J, Pérez-Juste J, García de Abajo F J and Liz-Marzán L M 2006 Seeded growth of submicron Au colloids with quadrupole plasmon resonance modes *Langmuir* **22** 7007–10
[34] Hurst S J, Lytton-Jean A K R and Mirkin C A 2006 Maximizing DNA loading on a range of gold nanoparticle sizes *Anal. Chem.* **78** 8313–8
[35] Krpetić Ž, Singh I, Su W, Guerrini L, Faulds K, Burley G A and Graham D 2012 Directed assembly of DNA-functionalized gold nanoparticles using pyrrole–imidazole polyamides *J. Am. Chem. Soc.* **134** 8356–9
[36] Jung H Y, Park Y-K, Park S and Kim S K 2007 Surface enhanced Raman scattering from layered assemblies of close-packed gold nanoparticles *Anal. Chim. Acta* **602** 236–43
[37] Le Ru E C, Galloway C and Etchegoin P G 2006 On the connection between optical absorption/extinction and sers enhancements *Phys. Chem. Chem. Phys.* **8** 3083–7
[38] Kleinman S L, Sharma B, Blaber M G, Henry A I, Valley N, Freeman R G, Natan M J, Schatz G C and Van Duyne R P 2013 Structure enhancement factor relationships in single gold nanoantennas by surface-enhanced raman excitation spectroscopy *J. Am. Chem. Soc.* **135** 301–8
[39] Bastus N G, Comenge J and Puntes V 2011 Kinetically controlled seeded growth synthesis of citrate-stabilized gold nanoparticles of up to 200 nm: size focusing versus ostwald ripening *Langmuir* **27** 11098–105
[40] Njoki P N, Lim I I S, Mott D, Park H-Y, Khan B, Mishra S, Sujakumar R, Luo J and Zhong C-J 2007 Size correlation of optical and spectroscopic properties for gold nanoparticles *J. Phys. Chem.* C **111** 14664–9
[41] Pazos-Perez N, Garcia de Abajo F J, Fery A and Alvarez-Puebla R A 2012 From nano to micro: synthesis and optical properties of homogeneous spheroidal gold particles and their superlattices *Langmuir* **28** 8909–14